Taylor & Francis
Taylor & Francis Group

Electric Power Components and Systems

ISSN: (Print) (Online) Journal homepage: https://www.tandfonline.com/loi/uemp20

Internet of Things-Based Induction Motor Diagnosis Using Convolutional Neural Network

Mubaraali L, Kuppuswamy N & Muthukumar R

To cite this article: Mubaraali L, Kuppuswamy N & Muthukumar R (04 Aug 2023): Internet of Things-Based Induction Motor Diagnosis Using Convolutional Neural Network, Electric Power Components and Systems, DOI: 10.1080/15325008.2023.2217434

To link to this article: https://doi.org/10.1080/15325008.2023.2217434

Electric Power Components and Systems, 0(0): 1–12, 2023

ISSN: 1532-5008 print / 1532-5016 online
DOI: 10.1080/15325008.2023.2217434

Taylor & Francis
Taylor & Francis Group

Internet of Things-Based Induction Motor Diagnosis Using Convolutional Neural Network

Mubaraali L,[1] Kuppuswamy N,[2] and Muthukumar R[3]
[1]Department of ECE, SNS College of Engineering, Coimbatore, Tamil Nadu, India
[2]Department of Mechanical Engineering, KIT-Kalaignar Karunanidhi Institute of Technology, Coimbatore, Tamil Nadu, India
[3]Department of Electrical and Electronics Engineering, Erode Sengunthar Engineering College, Erode, Tamil Nadu, India

CONTENTS

Abstract—We experimented analyzing motor vibration with aid of Raspberry Pi when, at that time, the engine vibration was abnormal. The Pi signal is transmitted to a relay by the motor supply disconnection. The control unit, nevertheless, monitors and sends the data to the storage system in good form with proper temperature. A FO-PID controller is utilized to analyze the effects of IM due to harmonic current, vibration, and noise. The induction motor's response to harmonic and current fluctuations is stabilized by a FO-PID controller. The findings can be displayed on the mobile. The tests were carried out in a static state of vibration condition, and fast Fourier transformation is used to analyze the measured vibration data signals. The results of this model were based on the convolutional neural network (CNN), which considerably monitors early diagnostics of the vibration. With a maximum delay of around 1 s, the controller can forward cloud vibration data. Using the CNN model train to analyze the performance of the classification accuracy, the stored data are collected. This article offers a novel way of building tools for measuring vibration in real time based on the schematic architecture provided by the Python mode.

Keywords: induction motor, vibration sensor, micro-electromechanical systems sensor, convolution neural network, fast Fourier transform
Received 25 January 2023; accepted 19 May 2023
Address correspondence to Mubaraali L, Department of ECE, SNS College of Engineering, Coimbatore, Tamil Nadu, 641107, India. E-mail: mubaraalilphd@gmail.com

1. INTRODUCTION

In industry, rotating machines are an important factor in modern society. Bearings have a big impact on the efficiency and productivity of a rotating machine. Rotating devices, such as wind turbines, gears, etc., are used in many industrial applications. Bearings are typically under full loads [1]. This can gradually reduce the impact and lead to system failure. The industry does not want to stop production due to possible system failures. When they know the cause of failure, they can choose their defense quickly and carefully. Thus, the industry could be pushed aside due to huge losses from production interruptions [2]. Measurements are often obtained for each machine end, close to the bearings, horizontal, and vertical axis locations by the vibration sensor, which monitors machine condition. Vibration sensors may identify faults, such as bearing

faults, mechanical instability, eccentricity, and misalignment in milliampere seconds (mas). The source of the motor vibration is from motor base, bearing, broken rotor bar, two-line frequency, and motor imbalance [3]. It is very important to understand that vibration signals are always a combination of the forcing effect (source effect) and the transfer function effect (structural transmission path). The use of electric motors is continuously expanding, and condition monitoring of those motors is of the utmost importance [4]. Condition monitoring science is looking into automated computer circuits to exclude human experts from the condition monitoring process. However, the development of artificial intelligence to monitor the health of electric cars is still in its infancy, and a lot of work is needed to implement these techniques for traditional healthcare despite significant work in this area [4]. The structure of the induction motor (IM) is exposed in Figure 1.

The abnormal behavior of the motor is first identified by associating it with the vibration intensity limit [5]. An accelerometer is an attractive option for piezoelectric ceramic micro-electromechanical systems (MEMS) in the embedded field because of its small size, low energy, and low cost. The MEMS accelerometer is widely used for use in portable product devices such as smartphones and tablets. This method of improvement not only reduced the size and cost of the device but also increased the MEMS accelerometer with greater accuracy and performance. The accuracy and bandwidth of a MEMS sensor were depend on the structure of its sensor components. On the one hand, the high frequency of naturally sensitive components influences large bandwidth. In contrast, sensitivity is inversely proportional to the natural version class. The strategy of MEMS-based sensor systems rotates around the trade-off between accuracy and bandwidth. It is, therefore, important to study the dynamic nature of sensory components.

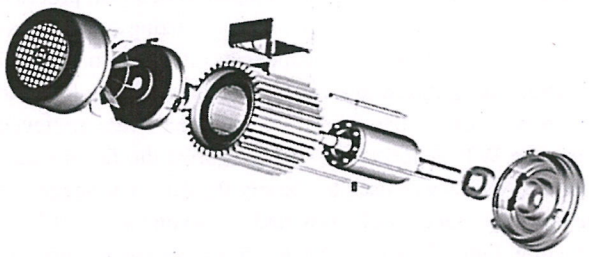

FIGURE 1. Construction of induction machine.

The dynamic and static properties of such components have been investigated in Figure 2 context of a variety of sandwich composites, nanostructures, microstructures, and carbon nanobuses. The small MEMS AC accelerometer makes it easy to connect small objects without affecting the mechanical properties of the test device. In addition, the multi-agent system charge amplifier (MAS CA) accelerometer requires fewer data acquisition components than a power amplifier-based system. Most modern MEMS can be connected directly to cheap microcontrollers *via* a serial data bus. In addition, MEMS accelerometers can usually retrieve data on acceleration along multiple axes at the same time, which enables three-dimensional movements to be registered. MEMS accelerometers are used in a variety of measurement schemes, including shock quantification. vehicle monitoring, rotating machines' vibration analysis, and motion and gesture recognition. Vibration detection or

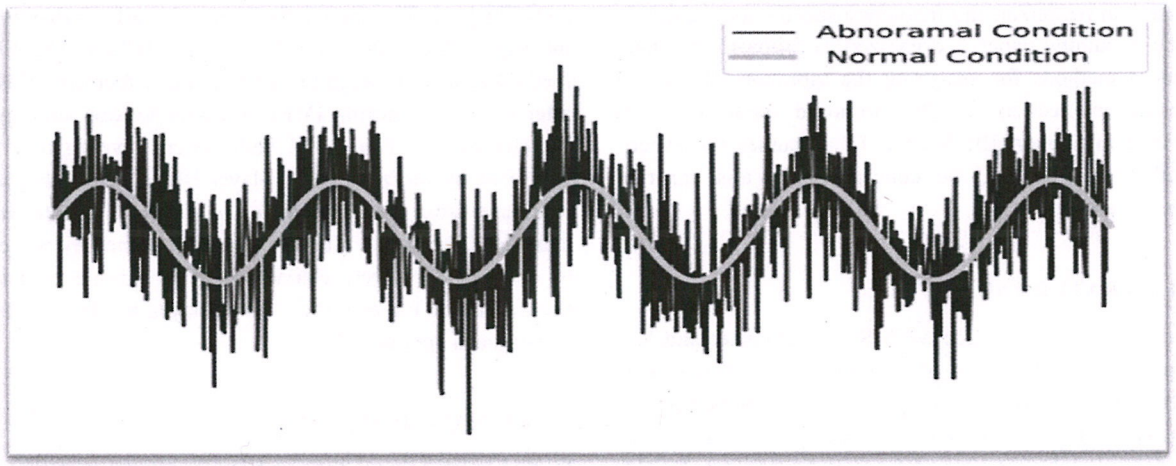

FIGURE 2. Representation of normal and peak vibration effects.

monitoring helps to discover any kind of unwanted vibration present in the motor, so the issue can be present at that time. In existing, there is a lot of existing technology to find faults in machines using the IoT. But until now, some drawback occurs in that existing model, so we planned to find vibration in the motor by using IoT. Here, we mainly used Raspberry Pi, which is already used in several IoT real-time projects. The major advantages of this device are simplicity in size, low cost, and the benefit of several interface ports. Analytical expression of vibration was developed for spline engines. The above problem makes it more important to reduce harmonics for IM with proportional integral derivative (PID) controllers. It is not easy to obtain alternating current (alternating current) at operating frequency for motor control, especially for IM with a conventional PID controller. Stability is ensured by active control of high-precision rotary motors, which improves motor efficiency. Full-order PID (IO) and PID (FO) controllers are already widespread in the industry. The tuning techniques of FO P I $\lambda D\mu$ controllers have been presented. To address and diagnose the mechanical problems of the IMs, vibration analysis is presented in this paper. The very fault operations of the adjustable speed drives often make the infrequent voltage content for the IMs inputs. The imbalance in voltage is caused by the single-phase load in three phase-based power systems. The main contributions are highlighted as follows:

- Analysis of vibration for the IM is examined and diagnosed using the convolutional neural network (CNN) method.
- The capacity to accurately evaluate the vibration data is necessary for the machinery diagnostic performed by vibration analysis to be accurate. For the vibration data, in particular, the frequency spectra are evaluated.

The remaining paper is organized as follows: The state-of-the-art methods for analyzing the vibration of IMs are discussed in Section II. The proposed methodology is described in Section III; Section IV discusses the experimental results; finally, the conclusion for this paper is given in Section V.

2. LITERATURE SURVEY

Introduced the open-source MEMS accelerometer and battery-powered IoT Memsio, it is a sensor unit that can be used to sense and measure a wide variety of movements. It is managed through a web browser [6], so it can be accessed remotely *via* a smartphone and computer. In addition, the results showed that Memsio can measure accurately and reliably. Memsio's operating time is about one business day, depending on the time it takes to measure and the frequency of these measurements, which is very large to finalize the value of it. In this study, we have significantly diagnosed the vibration in the motor in real time by using Raspberry Pi.

For classification purposes, we use the K-nearest neighbor (K-NN). The result of this research is the development of embedded systems to classify various failures in the machine. This experiment is performed on a testing facility in the mechanical vibration lab of the department of MED [7]. The total accuracy of our experiment is 91.5%, which is very less to analyze the behavior of the vibration sensors.

In the field of mechanical condition monitoring, diagnosis of faults in bearing is a hot topic. From examining data, feature extraction and classification of pattern are the crucial stages in bearings defect diagnosis. In the event that one or more bearing components fail, the bearings will vibrate more. The additional vibration frequency and the velocity of bearing are connected *via* the fault characteristic frequency. The HHT, the WT, EMD, and other methods were used for feature extraction in conventional methods of signal processing for the detection of bearing fault by utilizing signal vibrations [8]. The frequency components of the initial signal vibration are analyzed to identify the failing bearing [9]. The feature vectors of the accelerometer signal were retrieved using the WT. After training to categorize the feature vectors, the ANFIS was used to classify the data. The suggested method was successful even under varying load [10]. In detecting fault diagnosis, SVMs were employed successfully. The extraction of feature vectors with CWT, and the data examining for the three-phase IM was categorized using an SVM [11]. To identify the bearing's early problems, an intelligent defect detection based on a BPNN. The EMD method is used to acquire intrinsic mode functions (IMFs) after initially acquiring IMFs by decomposition strategy of wavelet packet. The signal fault pattern investigation was identified by utilizing a three-layer BPNN. Fault diagnosis was done using the Bayes net classifier and the naïve Bayes classifier. The signal vibrations were examined by wavelets to obtain the discrete characteristics of wavelet and then used as input for classification of Bayes net by suggested technique is applied [12].

3. PROPOSED METHOD

In this section, we discussed the projected technique in diagnosis of motor vibration. In this experimentation, we

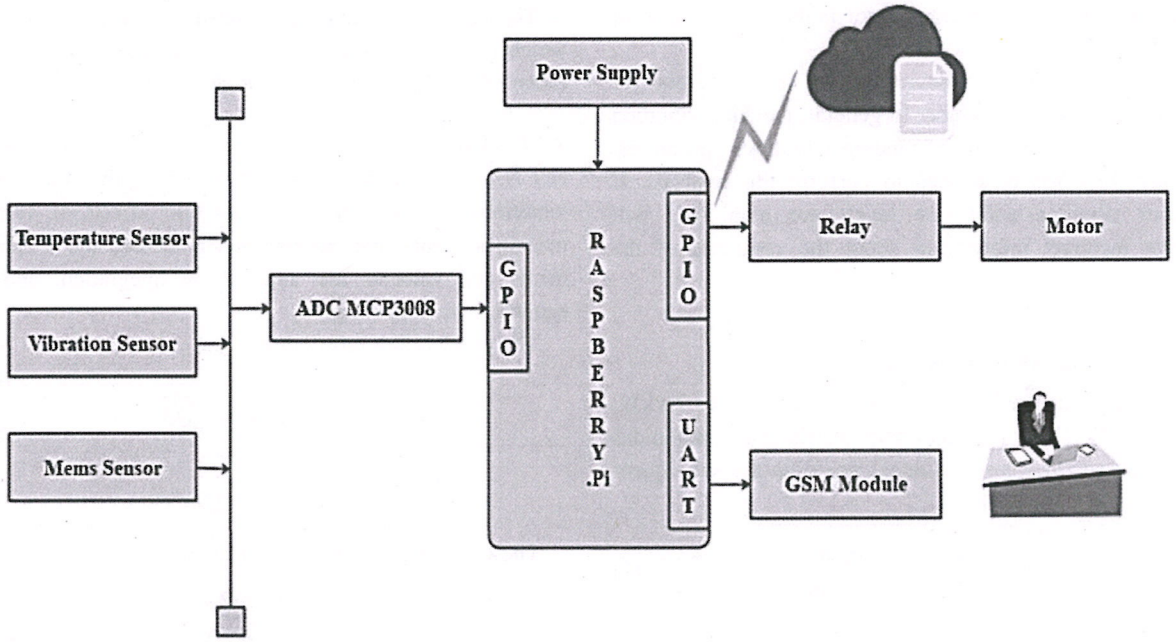

FIGURE 3. Proposed block diagram.

have proposed a method used to analyze the motor is monitored and controlled using an IoT system. In this study, we offered CNN-based monitoring and controlling scheme for recording the vibration, temperature, and angle of the vehicle. In this case, a power supply of 5 V DC is applied to turn ON the Raspberry Pi circuit. A Raspberry Pi microcomputer is the heart of the system; the vibration, temperature, and angle of the vehicle are collected by Raspberry Pi using sensors; the data is used to make a CNN model.

The system consists of sensors, an alert light-emitting diode (LEDs), a relay, a Global System for Mobile Communication (GSM) module, and a motor. The system is monitoring the vibration of the motor and controls. In this method, we have used three sensors as temperature, vibration, and MEMS sensors. The MEMS sensor is used as the ultralow-power for low, *i.e.*, 23 μA for the measurement mode and also 0.1 μA in the stand mode. An analog-to-digital converter (ADC) MCP3008 of 8-channel 10-bit used to convert the sensor output analog signal. This converter through the general-purpose input/output (GPIO) interface is connected to Raspberry Pi. The relay module is used to break the supply to the motor, when vibration is apart from normal, that time message will be transmitted to the user by using the GSM module. Then, the vibration and breaking values are stored in the cloud by using the Python tool when the Raspberry Pi was used to preprocess all the collected data and sent automatically to the database for future to learn the CNN model by automatically breaking the supply to the motor. The performance metrics are obtained by using the Python tool.

Figure 3 provides the block diagram for the proposed architecture. The vibration sensor comprises a MEMS sensor (ADXL345) and a small, thin, high-resolution ultrasonic accelerometer. It measures static acceleration applications as well as dynamic acceleration due to movement or impact. The analog device sensor signal works in analog-digital form and uses a capacitive measurement method in which the capacitance between the pin beam and the adjacent boom changes due to the weight of the load.

3.1. Vibration Diagnostics

The different experimental tasks include diagnostic vibration and vibration control. Vibration in the damaged zone determines the power deficiency during vibration diagnosis, and the force lines selection is related to speed. Diagnostics are generally measured in a narrow, low-frequency band, both velocity, and acceleration of the vibration. Most vibration measures are often taken with the use of piezoelectric vibration acceleration sensors. The energy

supply for the electric charge sensor is the output signal of this sort of sensor.

A vibration analysis device is an essential tool for detecting faults in a machine. In general, machine vibration is a static signal made up of random vibrations and noises. Usually, FFT has been used to perform this analysis. If random vibration and noise levels are high, you will receive incorrect information about the condition of the machine.

3.2. Induction Motor Vibration

This experiment used different ratings as 3.7 kW, 7.4 kW, and 14.7 kW IMs. The harmonic instruments amplitudes for the tested IM were considered based on the subsequent equations,

$$f(Hz) = \left(\frac{N}{2}\right) f_r \left[1 - \frac{b_d \cos(\beta)}{d_p}\right] \tag{1}$$

$$f(Hz) = \left(\frac{N}{2}\right) f_r \left[1 + \frac{b_d \cos(\beta)}{d_p}\right] \tag{2}$$

$$f(Hz) = d_p f_r / b_d \left[1 - \frac{b_d \cos(\beta)}{d_p}\right] \tag{3}$$

For a train defect,

$$f(Hz) = f_r/2) \left[1 - \frac{b_d \cos(\beta)}{d_p}\right] \tag{4}$$

where

- f_r is identified as rotational frequency;
- d_p is identified as diameter of ball pitch;
- b_d is identified as the diameter of ball;
- N is identified as the sum of balls;
- β is identified as the ball contact angle.

The analysis of vibration spectrum is used to determine the angle and temperature. The mistakes in vibration are defined by the two-value association, the amplitude of the harmonic components acquired from an observation of the vibration spectrum, and the harmonic mechanism's amplitude at the equivalent frequency from the spectrum of the position. This frequency of oscillation in the prevailing spectrum, that is.

$$f_{rul} = \lfloor f_1 \pm f_v \rfloor \tag{5}$$

where $k = 1, 2, 3, 4 \ldots$ and f_v is the characteristic of the frequencies of vibration.

The harmonic spectrum is constructed using FFT data, which is a mathematical process that extracts the representation of the frequency of a time domain signal.

3.2.1. Design of Accelerometer Vibration. The accelerometer is a widely used device for measuring the vibration of vibrations and recording the vibration effects of various machines. From the accelerometer record, the displacements and velocity are attained by integration, and its equations are following,

The acceleration ratio is given as

$$\frac{1}{[(1 - r^2)^2 + (2\xi r)^2]^{\frac{1}{2}}} \tag{6}$$

$$[(1 - r^2)^2 + (2\xi r)^2]$$

The operating speed can be written as

$$\omega = \frac{Rpm(2\pi)}{Time} \tag{7}$$

The accelerometer damped frequency as

$$\omega_d = \sqrt{1 - \xi^2 \omega_n} \tag{8}$$

$$\frac{\omega}{\omega_d} = \frac{\omega}{\sqrt{1 - \xi^2 \omega_n}} = \frac{r}{\sqrt{1 - \xi^2}} \tag{9}$$

$$r = \frac{\omega}{\omega_d} \sqrt{1 - \xi^2} \tag{10}$$

By taking ξ, the accelerometer undamped natural frequency as

$$\omega_n = \frac{\omega_d}{\sqrt{1 - \xi^2}} \tag{11}$$

Since, $\omega_n = \sqrt{k/m}$

$$k = m\omega_n^2 \tag{12}$$

The damping constant can be written as

$$c = 2m\omega_{n\xi} \tag{13}$$

3.2.2. Design of Vibrometer Calculation. This device consists of a cage mass meter, a K spring, and a crossed C connected to an oscillating body. With this arrangement, the ends of the spring and the dashboard trim and their vibrations move in the same way that the suspended mass moves. Then, the displacement of the mass with respect to the cell $z = x - y$, where x is the vertical displacement

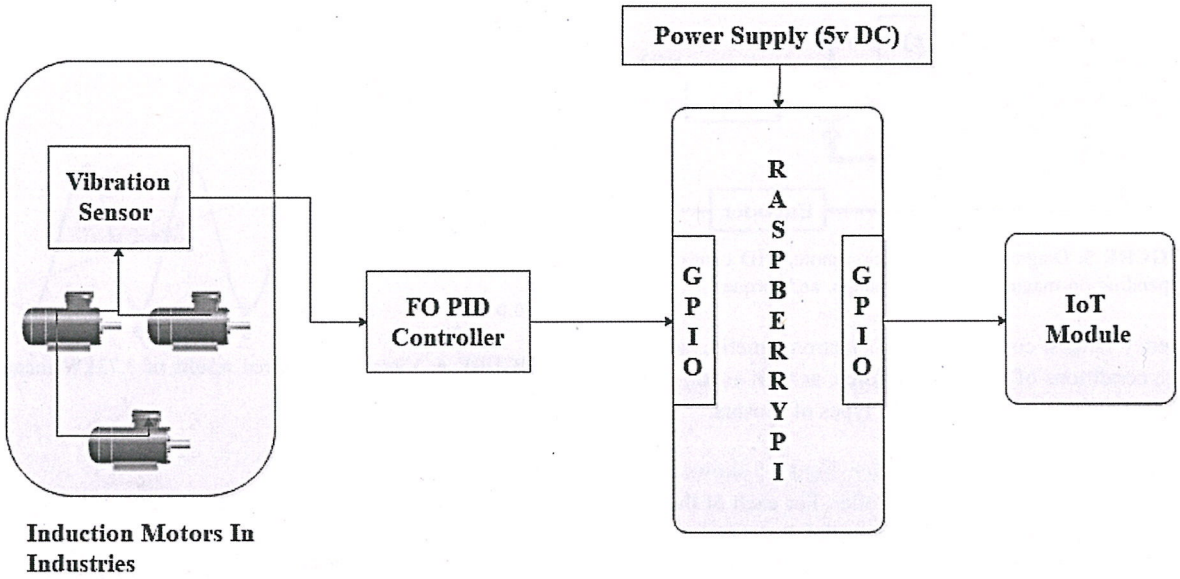

FIGURE 4. Proposed vibration controller architecture.

of the suspended mass, can be calculated using the following equation,

Assumed harmonic motion of vibration body

$$y(t) = Y sin\omega t \tag{14}$$

The mass can be written as

$$mx + c(x - y) + k(x - y) = 0 \tag{15}$$

The relative displacement z as

$$z = x - y \tag{16}$$

$$mz + cz + kz = my \tag{17}$$

$$mz + cz + kz = m\omega^2 Y \sin\omega t \tag{18}$$

The steady-state solution is given by,

$$z(t) = Zsin(\omega t - \emptyset) \tag{19}$$

where Z and Ø are given by

$$Z = \frac{Y\omega^2}{[(k - m\omega^2)^2 + c^2\omega^2]^{1/2}} = \frac{r^2 Y}{[(1 - r^2)^2 + (2\xi r)^2]^{1/2}} \tag{20}$$

$$\phi = \tan^{-1}\left(\frac{c\omega}{k - m\omega^2}\right) = \tan^{-1}\left(\frac{2\xi r}{1 - r^2}\right) \tag{21}$$

$$r = \frac{\omega}{\omega_n} \tag{22}$$

$$\xi = \frac{c}{2m\omega_n} \tag{23}$$

Therefore, the relative displacement between the mass and the base is essentially the same as the displacement of the base.

$$z(t) \cong Ysin(\omega t - \emptyset) \tag{24}$$

$$\frac{1}{[(1 - r^2)^2 + (2\xi r)^2]^{1/2}} \approx 1 \tag{25}$$

With $y(t) = Y sin\omega t$ shows that $z(t)$ gives rectilinear motion y (t) with the exception of the phase delay. The distance between these phases can be considered equal to 180, equal to $\xi = 0$. If the displacement thus recorded by y (t) is delayed with respect to the time to measure the z (t) offset, then there is no interval at that time if the base offset y (t) has a single harmonic element.

Figure 4 shows the proposed vibration controller architecture for controlling motor vibration in industries. In this technique, we identified the vibration in both load and unload conditions of motors, and also, here, we mentioned three kinds of IMs used to analyze and control the vibration using the FO PID controller. The vibration sensor sensitivity of (±10%) and frequency range of (±3dB) are computed. In order to receive important operating information *via* sensors, the motor works in a safe environment for the person working on the machine. Different conditions associated with extreme temperatures, magnetic fields, vibration ranges,

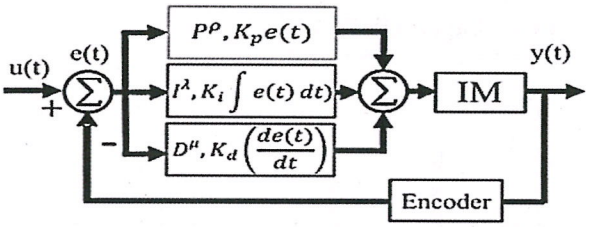

FIGURE 5. Diagram of an induction motor PID controller depending on magnetic current, voltage, and torque.

frequency ranges, compatibility of electromagnetic, and discharge conditions of electrostatic force, as well as the essential signal quality, require different types of sensors.

3.2.3. Scheme of FO PID Controller. Figure 5 shows a control scheme with the FO PID controller. For each of the considered parameter projects, the controller P depends on the current, so that the same output signal relative to the error E(T) current is generated. The P-controller upsurges the standard slew rate for current and voltage. Adjust the error condition to stable state until the error condition is zero by using the I-controller. On the other hand, the I-controller also confines response rates and disturbs system stability.

Controller D by future errors prediction solves this problem. Controller D can develop system stability by changing the phase delay state. If the controller parameter D is increased, the motor closed loop has an acceptable speed to reach its reference. However, most D controllers will over-respond to the motor and exceed the limit. The stability and efficiency of active IM control can be enhanced. A master controller is required to compensate for the delay in phase. This study improves the FO PID controller to recover the robustness and stability margins of the IM system compared to the broadly used traditional PID controller. The FO PD controller μ may be appropriate and is also economical. However, by utilizing FO-PID-μ controller, there is still a static position error due to several kinds of integral terms. To solve this problem, an FO-PID controller is proposed, but FO-PID $\lambda D\mu$ does not act as a PID controller for IM control. Project factors as follows

$$u(t) = K_P^p e(t) + K_i^{\lambda} \int_0^t e(t)dt + K_d^{\mu} \frac{de(t)}{dt} \qquad (26)$$

where E (T) represents an error value, proportional gain represents a genetic component, that represents an integral component, and K represents a derivative component. ρ, λ, and μ cannot be positive integers. The PID controller function provides a control value of U for most preprocesses. In general, tuning methods of parameter for Pρ I $\lambda D\mu$ controllers can be logically obtained by solving non-linear devices and satisfying the phase transition frequency and vector space between gain position and edge settings.

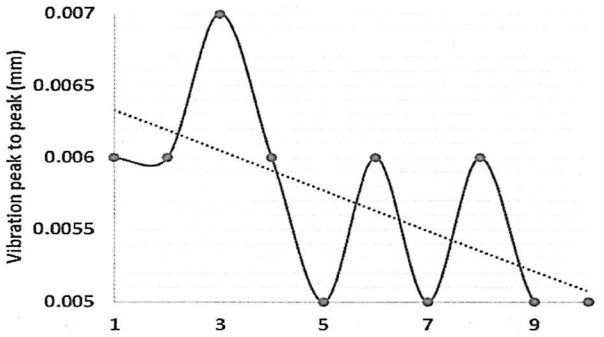

FIGURE 6. Vibration measured results of 3.73 kW induction motor.

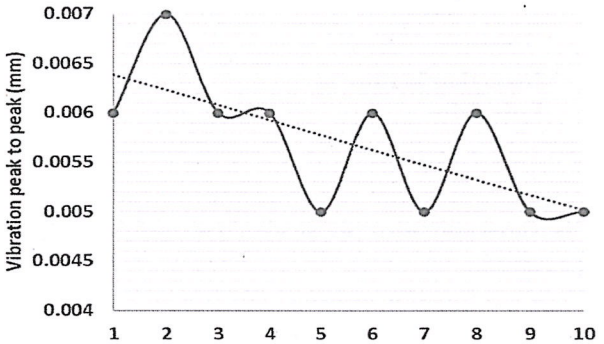

FIGURE 7. Vibration measured results of 7.4 kW induction motor.

The consequences of the PID vector vibration control for driving IMs are also presented. The analysis of IME domain regulates the effect of changing PID controller operating factors on vibration and noise.

Figures 6, 7, and 8 show that the investigational consequences show a case study of the vibration characteristics for three types of rotary IMs. Measurements show that PID-controlled asynchronous drives can reduce motor-generated noise and vibrations. The results of the motor speed experiment show that a higher speed (1200 rpm) is applied to the IM. This is greater than the low-speed IM (500 rpm) because the PID controller has an unbalanced current.

According to the graphical results plotted in Figure 9, the vibration rate is not increased when the load is passing into it. For the two distinct situations, such as those with and without a load. In this instance, both the load and the motor's speed are altered. As a result, the significance of the vibration rate in relation to speed is examined.

3.2.4. Comparison of PID Controller and FO PID Controller Performance. The vibration suppression effect of an IM is compared to separating the PID controller and

the conventional PID controller. The different speeds of spectrum vibration and the spectrum stator current of the motor are analyzed and compared. The FO-PID controller's vibration suppression provides improved performance on comparing with conventional PID controller.

The spectrum data on stable functioning below 450, 600, and 750 rpm are compared and analyzed in Table 1. The FO-PID controller has some advantages over the vibration suppression efficiency of the FPID controller.

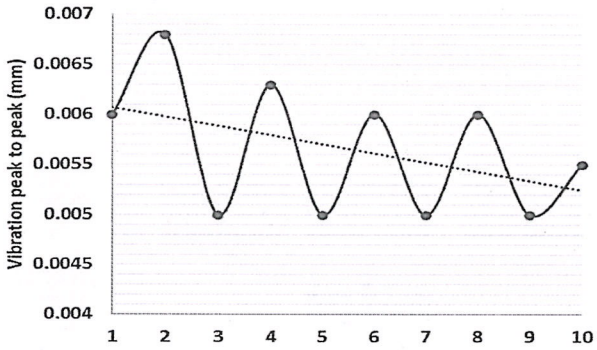

FIGURE 8. Vibration measured results of 14.7 kW induction motor.

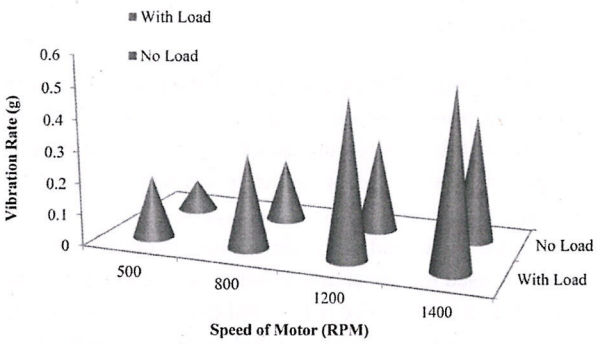

FIGURE 9. Vibration rate for speed of motor.

		PID controller		FO PID controller	
Data type	Speed rpm	3.4 kHz spectrum peak value	6.8 kHz spectrum peak value	3.4 kHz spectrum peak value	6.8 kHz spectrum peak value
Vibration frequency (mg)	450	63.64	25.54	36.62	14.74
	600	72.93	22.61	52.47	19.35
	750	138.71	18.08	69.19	13.44

TABLE 1. Comparisons of two controller performances of vibration and current ratio under the diverse speed.

4. RESULTS AND DISCUSSION

We evaluate vibration diagnostic performance; experiments are done with 4GB RAM, I5 Processor, and 1GB hard drive using Python tool 3.6.8. With the measurement of the angle, vibration, and temperature of the motor, we analyze the efficiency diagnostic of vibrations in different loads. Here, the performance of classification was calculated with the confusion matrix.

The derived data of phase 2 from the piezoelectric accelerometer are presented in Figure 10. A piezoelectric accelerometer is fitted to the electric machine chassis. The analysis of transmitted vibration signals is, therefore, very important.

Figure 11 shows the analyzed frequencies F1 and F2 for amplitude vibration, and sideband 150–3 Hz is greater than the same motor.

It is very important to analyze the vibration magnitude, as a variance of more than 11% can indicate a trick.

In Table 2, we analyze the temperature and vibration in normal and peak conditions of the motor.

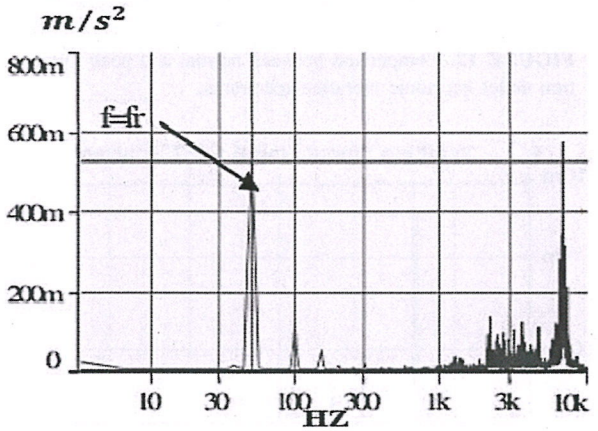

FIGURE 10. IM harmonic vibration spectra with normal vibration condition.

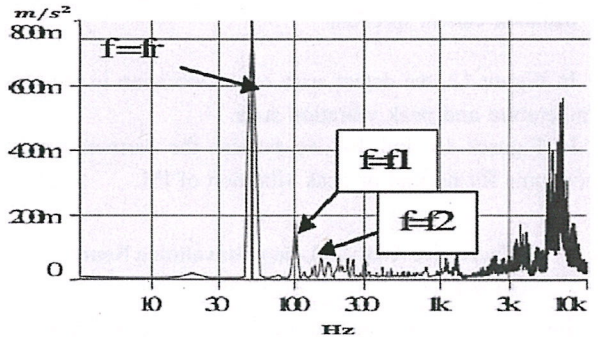

FIGURE 11. IM harmonic vibration spectrums at peak vibration condition.

		f1{Hz} 100	f2{Hz}	Average (150-300)Hz
Normal condition	Vibration amplitude [mm/s^2]	0.11	0.040	0.050
Peak condition	Vibration amplitude [mm/s^2]	0.18	0.055	0.069

TABLE 2. Vibration analysis in peak and normal conditions.

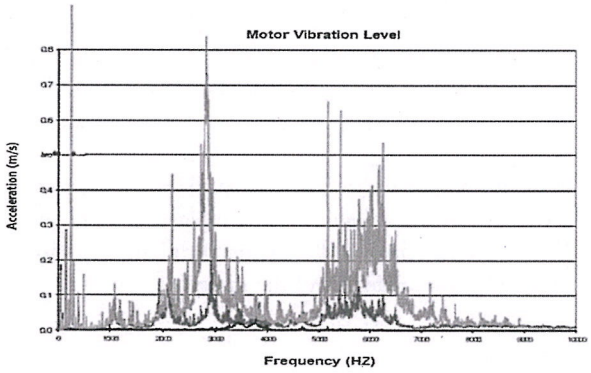

FIGURE 12. Comparison between normal and peak vibration under harmonic vibration spectrums.

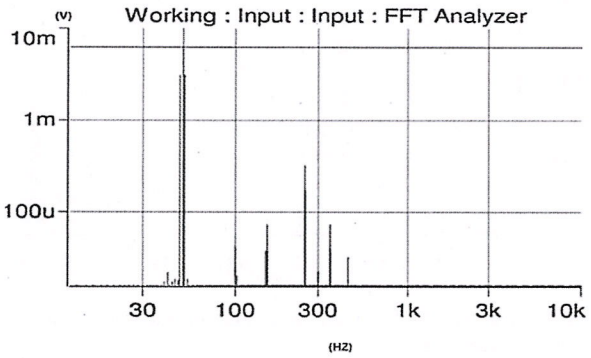

FIGURE 13. IM with normal vibration condition under harmonic current spectrum.

In Figure 12, we detect arise of the vibration in the high temperature and peak vibration state.

In Figures 13 and 14, we present the harmonic noise spectrums for normal or peak vibration of IM.

4.1. Performance Analysis Using Convolution Neural Network

In this section, we conducted the deep learning technique of CNN used to analyze the performance measure. Initially, the sensor data are in nature of the analog signal, converted to

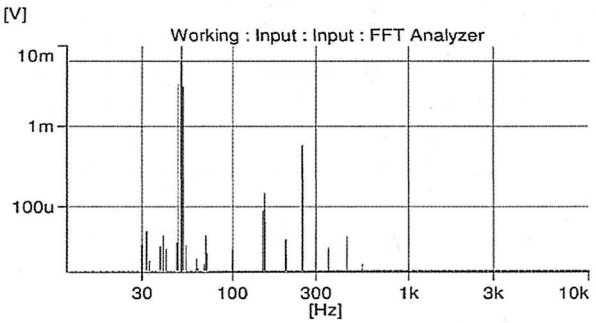

FIGURE 14. IM with peak vibration condition under harmonic current spectrum.

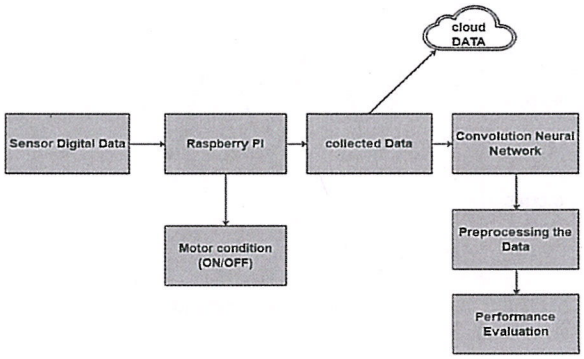

FIGURE 15. Performance evaluation of CNN by using cloud-stored data.

the digital signal, and then given to the Raspberry Pi, which controls the motor vibration and decision to ON/OFF the motor. When vibration occurs under abnormal conditions, it will operate the relay to disconnect motor supply, but if the motor operating at normal vibration speeds, it monitors the temperature, angle, and vibration of the motor. The Python software is used to collect and monitor data to store it in the cloud. That cloud-recorded file is used to train the neural network to analyze the performance and great work in the kind of robotically. This technique is used to safeguard from minor or major damage to the motor. In Figure 15, the sensor data are used to train and analysis the performance of CNN.

4.1.1. Convolution Neural Network. CNN with multiple layers such as the pooling, ReLU, and fully connected layer. The feature of the images is mainly identified by using CNN to find the image edge and shape.

4.1.2. Convolutional Layer. In CNN architecture, the approach of first-come, first-served is usually complicated. Normally, CNN accepts the input level of MxNx1. Here are the different levels of MxN vibrational data. CNN utilizes filters

that are equally valid for the data and are inserted into the filtered data with certain parameters. The process of convection can be equated (27).

$$s(t) = (x^* w)(t) \tag{27}$$

4.1.3. Pooling Layer. To reduce the data size, this layer is designed. The organization of the matrix data in various parts and the whole segment is grouped into a single value, lowering the dimensions of the metric data. Some prominent pooling characteristics are the max pool and the average pool when all arrays in the current layer change to the average or high level. In this layer, the vibration frequency is computed with reference to the number of occurrences of the periodic event per time, and also it is estimated using cycles/seconds. In this case, 1 cycle requires 2 s to complete, and also the frequency of the 1 cycle is 2s representing the vibration frequency of 0.5 Hz.

4.1.4. Fully Connected Layer. These layers have been modified to fit the architecture at the network level. A fully linked layer is a working action between a meter and N in which the input and output parameters are connected. This layer connects all action from the previous layer to the next network level, just like a classic artificial nerve network in general.

4.1.5. Softmax Layer. Softmax turns the previous levels' inputs into class probabilities. That level, therefore, plays a critical influence in the output, because the most probability for given inputs is the forecasted output class. In particular, assume that the input is Xji for that this softmax layer computes the output, and also Ej represents the vibration sensor features extracted in the fully connected layer; finally, the predicted probability is computed as follows,

$$\tilde{Y}_j^i = \frac{1}{1 + \exp\left(-w^t.\delta_j + b\right)} \text{ where } \delta_j = \left[\hat{X}_j^1, \hat{X}_j^2 \ldots \hat{X}_j^M, e_j\right] \tag{28}$$

Here, w is the learnable weight value, and this is the value prediction problem; thus, it increases with the $1 - \hat{Y}_j$

4.2. Preprocessing

Preprocessing is the important technique for raising the caliber of the cloud data stream. The SNR and data amplitude have been reduced by the implementation of many process stages, including the elimination of data artifacts on the input signal. The subsequent steps involve the selection of the vibrational signal is also a part of the preprocessing phase.

4.3. Training and Classification

Based on the CNN algorithm, a two-level classification is used to determine the vibration of the engine and its intensity. Of the selected subsets of functions for each load level, the entire test data set is classified based on engine vibration. The former uses the entire training set to train CNN, while the latter uses the training data for vibration, temperature, or motor angle from the CNN classifier. Using the training set, the grid search returns twice the accuracy of cross-validity, where the accuracy of cross-validity is the percentage of accurately classified data. Then, the values that correspond to the best cross-validity accuracy are selected. The entire training dataset is retrained with optimal parameters to define the CNN classification. They trained the information backward propagation algorithm in a multi-layer network propagation feed forward, is a self-organized network with a 2D map functions. The input stator current of the neural network and/or the motor vibration frequency are typical.

The evaluation metrics are utilized to measure the effectiveness and classification of our technology as (0, 50, or 100) percent in various load conditions. For the classification, parameters for evaluation includes precision (P), specificity (SP), sensitivity (SE), and accuracy (AC). The performance measures parameter as follows:

$$P = \frac{tp}{tp + fP} \tag{28}$$

$$SE = \frac{tp}{tp + fn} \tag{29}$$

$$SP = \frac{tn}{tn + fp} \tag{30}$$

$$\text{AC} = \frac{tp + tn}{tp + fp + tn + fn} \tag{31}$$

where tp, tn, fp, and fn signify the sum of predicted circumstances, which are exemplified as true positive and negative, false positive and negative.

The performance of classification of vibration diagnostics in different load conditions was shown in Table 3 and Figure 16. It has an accuracy of 96% and a sensitivity of

Classification model	Load condition (%)	Specificity	Precision	Sensitivity	Accuracy
CNN	0%	85%	89%	90%	96%
CNN	50%	90%	86%	88%	94%
CNN	100%	87%	87%	86%	93%

TABLE 3. Performance analysis of the proposed model under various loads.

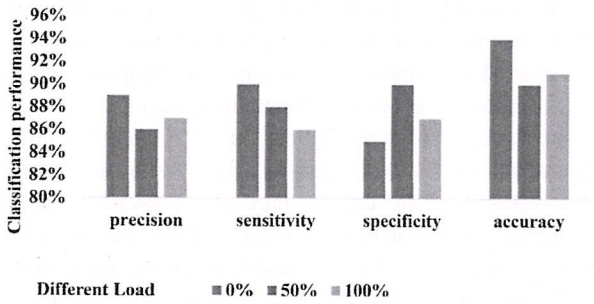

FIGURE 16. Classification performance under different load conditions.

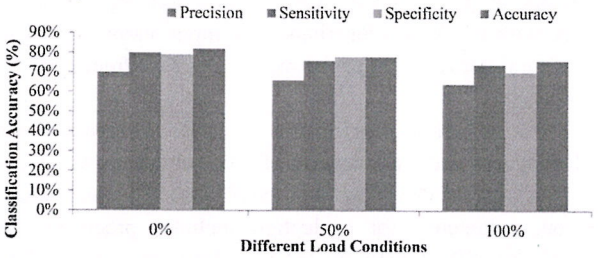

FIGURE 17. Classification performance under different load conditions (DNN).

90% when there is no load. Additional 50% of the load conditions, 90% of the specificities and accuracy, followed by 100% of the loads, 87% of the accuracy, and 93% of the classifications performance have achieved the accuracy, while the classification of vibration diagnostics in various load conditions for ongoing work has accomplished the accuracy, *i.e.*, DNN deep learning model was shown in Figure 17.

5. CONCLUSION

We proposed a new methodology for diagnosing vibrations in an IM in this version at an early stage without significant motor damage. The approach provided is IoT controller-based on the of Raspberry Pi and evaluating the performance by utilizing a deep neural network based on CNN. The FO PI controller can increase the induction engine performance, based on design trials. The frequencies of vibration are analyzed using FFT and CNN. In experimental results that compared a classification with a typical under various stress settings, the approach proposed has the maximum detection and the least false rate. Experimental results reveal a considerable increase in efficiency and intensity in the proposed two-tier classification. In our proposed solution, when peak vibration is in the engine, it can automatically turn away from the engine. At that time, the proposed model can communicate to senior industry managers and also alert industry personnel. The data are safely kept by the Python idle tool on the cloud. These data are utilized to diagnose the performance of the suggested model. In this study, we employ CNN, based on the technology of a deeper learning concept. The description of a neural network-based diagnostic approach makes it clear that much work has to be done before the neural network can be developed, and its learning process can be used, but the findings are successfully used in the industry. Finally, this experimental result proved that the proposed technique was a better vibration diagnosis scheme in real-time application.

DISCLOSURE STATEMENT

Conflict of interest is not applicable in this work.

ETHICS APPROVAL AND CONSENT TO PARTICIPATE

No participation of humans takes place in this implementation process

HUMAN AND ANIMAL RIGHTS

No violation of Human and Animal Rights is involved.

DATA AVAILABILITY STATEMENT

Data sharing not applicable to this article as no datasets were generated or analyzed during the current study

REFERENCES

[1] R. M. Souza, E. G. Nascimento, U. A. Miranda, W. J. Silva, and H. A. Lepikson, "Deep learning for diagnosis and classification of faults in industrial rotating machinery," *Comput. Ind. Eng.*, vol. 153, pp. 107060, Dec. 2021. DOI: 10.1016/j.cie.2020.107060.

[2] W. Ahmad, S. A. Khan, M. M. Islam, and J. M. Kim, "A reliable technique for remaining useful life estimation of rolling element bearings using dynamic regression models," *Rel. Eng. Sys. Safety.*, vol. 184, no. 2, pp. 67–76, Jan. 2019. DOI: 10.1016/j.ress.2018.02.003.

[3] M. Baptista, S. Sankararaman, I. P. de Medeiros, C. Nascimento, H. Prendinger, and E. M. Henriques, "Forecasting fault events for predictive maintenance using data-driven techniques and ARMA modelling," *Comput. Ind. Eng.*, vol. 115, no. 1–2, pp. 41–53, Nov. 2018. DOI: 10.1016/j.cie.2017.10.033.

[4] W. Li, S. Gu, X. Zhang, and T. Chen, "Transfer learning for process fault diagnosis: knowledge transfer from simulation to physical processes," *Comput. Chem. Eng.*, vol. 139, pp. 106904, May 2020. DOI: 10.1016/j.compchemeng.2020.106904.

[5] Y. C. Chuang, T. Chen, Y. Yao, and D. S. H. Wong, "Transfer learning for efficient meta-modeling of process simulations," *Chem. Eng. Res. Des.*, vol. 138, pp. 546–553, Oct. 2018. DOI: 10.1016/j.cherd.2018.07.008.

[6] W. Zhang, G. Peng, C. Li, Y. Chen, and Z. Zhang, "A new deep learning model for fault diagnosis with good anti-noise and domain adaptation ability on raw vibration signals," *Sensors.*, vol. 17, no. 2, pp. 425, Feb. 2017. DOI: 10.3390/s17020425.

[7] Z. Zhang, X. Li, L. Wen, L. Gao, and Y. Gao, "Fault diagnosis using unsupervised transfer learning based on adversarial network," 2019 IEEE 15th Int. CASE, pp. 305–310, Sep. 2019. DOI: 10.1109/COASE.2019.8842881.

[8] Z. Wan, R. Yang, and M. Huang, "Deep transfer learning-based fault diagnosis for gearbox under complex working conditions," *Shock Vib.*, vol. 2020, no. 9, pp. 1–13, Nov. 2020. DOI: 10.1155/2020/8884179.

[9] Y. Lei, B. Yang, X. Jiang, F. Jia, N. Li, and A. K. Nandi, "Applications of machine learning to machine fault diagnosis: a review and roadmap," *Mech. Syst. Signal Process.*, vol. 138, pp. 106587, Apr. 2020. DOI: 10.1016/j.ymssp.2019.106587.

[10] P. Ghosh, S. Azam, A. Karim, M. Hassan, K. Roy, and M. Jonkman, "A comparative study of different machine learning tools in detecting diabetes," *Procedia Comput. Sci.*, vol. 192, pp. 467–477, Jun. 2021. DOI: 10.1016/j.procs.2021.08.048.

[11] P. Ghosh, S. Azam, K. M. Hasib, A. Karim, M. Jonkman, and A. Anwar, "A performance based study on deep learning algorithms in the effective prediction of breast cancer," 2021 IJCNN., pp. 1–8, Sept. 2021. DOI: 10.1109/IJCNN52387.2021.9534293.

[12] F. J. M. Shamrat, *et al.*, "Analysing most efficient deep learning model to detect COVID-19 from computer tomography images," *IJEECS.*, vol. 26, no. 1, pp. 462–471, Apr. 2022. DOI: 10.11591/ijeecs.v26.i1.pp462-471.

BIOGRAPHIES

L. Mubaraali presently working as Assistant Professor, Department of ECE, SNS College of Engineering, Sarvanampatty, Coimbatore. He received his B.E Degree in Electronics and Communication Engg. from Maharaja Prithivi Engineering College, Coimbatore, M.E., in VLSI DESIGN. From Regional centre Anna University, Coimbatore and Pursuing Ph.D in Information & Communication Engineering at Anna University, Chennai.

N. Kuppuswamy presently is working as Professor in Department of Mechanical Engineering KIT- Kalaignar Karunanidhi Institute of Technology in Coimbatore. He received his B.E Degree in Mechanical Engineering, PSG College of Technology, Coimbatore, M.E., in Production Engineering from PSG College of Technology, Coimbatore and completed Ph.D in Production Engineering from PSG College of Technology, in 2005.

R. Muthukumar presently working as Associate professor in Erode Sengunthar Engineering College, Erode. He received his B.E Degree in Electrical and Electronics Engg. from CIT, Coimbatore, M.E., in Power Systems Engg. From GCT, Coimbatore and completed Ph. D in Power System Engineering at Anna University, Chennai, in 2014. He has published more than eighteen international journals and has fifteen International/National conference publications. His research interest includes power system planning, voltage stability analysis and application of evolutionary algorithms to power system optimization.